Supporting Information (SI-1): "Detection and long-term quantification of methane emissions from an active landfill"

Pramod Kumar[1], Christopher Caldow[1,2], Grégoire Broquet[1], Adil Shah[1], Olivier Laurent[1], Camille Yver-Kwok[1], Sebastien Ars[3], Sara Defratyka[1,6], Susan Gichuki[1], Luc Lienhardt[1], Mathis Lozano[1], Jean-Daniel Paris[1], Felix Vogel[3], Caroline Bouchet[4], Elisa Allegrini[4], Robert Kelly[4], Catherine Juery[5], and Philippe Ciais[1]

[1]Laboratoire des Sciences du Climat et de l'Environnement (LSCE/IPSL), CEA-CNRS-UVSQ, Université Paris-Saclay, 91191 Gif-sur-Yvette, France
[2]Climate Science Centre, CSIRO Oceans and Atmosphere, Aspendale, VIC, 3195, Australia
[3]Climate Research Division, Environment and Climate Change Canada, Toronto M3H 5T4, Ontario, Canada
[4]SUEZ-Smart & Environmental Solutions, Tour CB21/16 place de l'Iris, 92040, La Défense, France
[5]TotalEnergies Laboratoire Qualité de l'Air (LQA), 69360 Solaize Cedex, France
[6]now at University of Edinburgh, United Kingdom and National Physical Laboratory, United Kingdom

Correspondence: Pramod Kumar (pramod.kumar@lsce.ipsl.fr)

Abstract. This supporting information material (SI-1) documents all the measurement campaigns conducted for leak detection and quantification of methane emissions from Butte-Bellot landfill.

List of Figures

S1.1 The development of the Butte-Bellot landfill as depicted in satellite imagery provided by Google Earth (©Google Earth). The years that each image was captured, progressing from left to right in each row, and from the top row to the bottom row, are: 2003, 2005, 2007, 2009, 2014, 2015, 2016, 2018, and 2020. These images suggest that the Eastern side of the landfill has been filled sequentially in three cells starting in the North-East (active 2005,2007) then progressing to the East (active: 2014, 2015) and finally the South-East (active since 2018 to 2020). 4

S1.2 (a) CH_4mole fraction time series from the mobile near-surface measurements and (b) wind conditions on **September 13, 2016**. Enhancement of CH_4mole fractions above the background in plume transects (c) & (d) along the near-landfill (ABCD) road. The distances along road segments are computed from A towards anticlockwise direction . Black lines in (c)-(d) show the averaged mole fractions computed from these multiple transects. 5

S1.3 (a) CH_4mole fraction time series from the mobile near-surface measurements and (b) wind conditions on **November 17, 2016**. Enhancement of CH_4mole fractions above the background in plume transects (c) & (d) along the near-landfill (ABCD) road. The distances along road segments are computed from A towards anticlockwise direction . Black lines in (c)-(d) show the averaged mole fractions computed from these multiple transects. 6

S1.4 (a) CH_4mole fraction time series from the mobile near-surface measurements and (b) wind rose on **December 05, 2016**. Enhancement of CH_4mole fractions above the background in plume transects along the first (c) & (d) and the second (e) & (f) remote roads. The distances along road segments are computed from E . Black lines in (c)-(f) show the averaged mole fractions computed from these multiple transects. 7

S1.5 (a) CH_4mole fraction time series from the mobile near-surface measurements and (b) wind conditions on **August 11, 2017**. Enhancement of CH_4mole fractions above the background in plume transects (c) & (d) along the near-landfill (ABC) road and (e) & (f) far-landfill remote road (EF). The distances along road segments are computed from A and E respectively for near-landfill (ABC) and far-landfill (EF) roads. Black lines in (c)-(f) show the averaged mole fractions computed from these multiple transects. 8

S1.6 (a) CH_4mole fraction time series from the mobile near-surface measurements and (b) wind conditions on **September 28, 2017**. Enhancement of CH_4mole fractions above the background in plume transects (c) & (d) along the near-landfill (ABC) road. The distances along road segments are computed from A towards anticlockwise direction. Black lines in (c)-(d) show the averaged mole fractions computed from these multiple transects. 9

S1.7 (a) CH_4mole fraction time series from the mobile near-surface measurements and (b) wind conditions on **October 06, 2017**. Enhancement of CH_4mole fractions above the background in plume transects (c) & (d) along the near-landfill (ABC) road and (e) & (f) far-landfill remote road (EF). The distances along road segments are computed from A and E respectively for near-landfill (ABC) and far-landfill (EF) roads. Black lines in (c)-(f) show the averaged mole fractions computed from these multiple transects. 10

S1.8 (a) CH_4mole fraction time series from the mobile near-surface measurements and (b) wind conditions on **July 26, 2018**. Enhancement of CH_4mole fractions above the background in plume transects (c) & (d) along the near-landfill (ABC) road and (e) & (f) far-landfill remote road (EF). The distances along road segments are computed from A and E respectively for near-landfill (ABC) and far-landfill (EF) roads. Black lines in (c)-(f) show the averaged mole fractions computed from these multiple transects. 11

S1.9 (a) CH_4mole fraction time series from the mobile near-surface measurements and (b) wind rose on **November 27, 2018**. Enhancement of CH_4mole fractions above the background in plume transects (c) & (d) along the near-landfill (ABC) road. The distances along road segments are computed from A. Black lines in (c)-(d) show the averaged mole fractions computed from these multiple transects. 12

S1.10(a) CH_4mole fraction time series from the mobile near-surface measurements and (b) wind rose on **January 10, 2019**. Enhancement of CH_4mole fractions above the background in plume transects (c) & (d) along the near-landfill (ABC) road and (e) & (f) far-landfill remote road (EF). The distances along road segments are computed from A and E respectively for near-landfill (ABC) and far-landfill (EF) roads. Black lines in (c)-(f) show the averaged mole fractions computed from these multiple transects. 13

S1.11(a) CH_4mole fraction time series from the mobile near-surface measurements and (b) wind conditions on **February 12, 2019**. Enhancement of CH_4mole fractions above the background in plume transects (c) & (d) along the near-landfill (ABC) road and (e) & (f) far-landfill remote road (EF). The distances along road segments are computed from A and E respectively for near-landfill (ABC) and far-landfill (EF) roads. Black lines in (c)-(f) show the averaged mole fractions computed from these multiple transects. 14

S1.12(a) CH_4mole fraction time series from the mobile near-surface measurements and (b) wind rose on **July 10, 2019**. Enhancement of CH_4mole fractions above the background in plume transects (c) & (d) along the near-landfill (ABC) road and (e) & (f) far-landfill remote road (EF). The distances along road segments are computed from A and E respectively for near-landfill (ABC) and far-landfill (EF) roads. Black lines in (c)-(f) show the averaged mole fractions computed from these multiple transects. 15

S1.13(a) CH_4mole fraction time series from the mobile near-surface measurements and (b) wind rose on **August 02, 2019**. Enhancement of CH_4mole fractions above the background in plume transects (c) & (d) along the near-landfill (ABC) road and (e) & (f) far-landfill remote road (EF). The distances along road segments are computed from A and E respectively for near-landfill (ABC) and far-landfill (EF) roads. Black lines in (c)-(f) show the averaged mole fractions computed from these multiple transects. 16

S1.14(a) CH_4mole fraction time series from the mobile near-surface measurements and (b) wind rose on **August 29, 2019**. Enhancement of CH_4mole fractions above the background in plume transects (c) & (d) along the near-landfill (ABC) road. The distances along road segments are computed from A. Black lines in (c)-(d) show the averaged mole fractions computed from these multiple transects. 17

S1.15(a) CH_4mole fraction time series from the mobile near-surface measurements and (b) wind rose on **September 13, 2019**. Enhancement of CH_4mole fractions above the background in plume transects (c) & (d) along the near-landfill (ABC) road and (e) & (f) far-landfill remote road (EF). The distances along road segments are computed from A and E respectively for near-landfill (ABC) and far-landfill (EF) roads. Black lines in (c)-(f) show the averaged mole fractions computed from these multiple transects. 18
S1.16(a) CH_4mole fraction time series from the mobile near-surface measurements and (b) wind rose on **December 09, 2019**. Enhancement of CH_4mole fractions above the background in plume transects (c) & (d) along the near-landfill (ABC) road and (e) & (f) far-landfill remote road (EF). The distances along road segments are computed from A and E respectively for near-landfill (ABC) and far-landfill (EF) roads. Black lines in (c)-(f) show the averaged mole fractions computed from these multiple transects. 19
S1.17(a) CH_4mole fraction time series from the mobile near-surface measurements and (b) wind rose on **February 05, 2020**. Enhancement of CH_4mole fractions above the background in plume transects (c) & (d) along the near-landfill (ABC) road and (e) & (f) far-landfill remote road (EF). The distances along road segments are computed from A and E respectively for near-landfill (ABC) and far-landfill (EF) roads. Black lines in (c)-(f) show the averaged mole fractions computed from these multiple transects. 20
S1.18(a) CH_4mole fraction time series from the mobile near-surface measurements and (b) wind rose on **March 04, 2020**. Enhancement of CH_4mole fractions above the background in plume transects (c) & (d) along the near-landfill (ABC) road. The distances along road segments are computed from A for near-landfill (ABC) road. Black lines in (c)-(d) show the averaged mole fractions computed from these multiple transects. 21
S1.19(a) CH_4mole fraction time series from the mobile near-surface measurements and (b) wind rose on **September 04, 2020**. Enhancement of CH_4mole fractions above the background in plume transects (c) & (d) along the near-landfill (ABC) road. The distances along road segments are computed from A for near-landfill (ABC) road. Black lines in (c)-(d) show the averaged mole fractions computed from these multiple transects. 22
S1.20(a) CH_4mole fraction time series from the mobile near-surface measurements and (b) wind conditions on **October 15, 2020**. Enhancement of CH_4mole fractions above the background in plume transects (c) & (d) along the near-landfill (ABC) road. The distances along road segments are computed from A for near-landfill (ABC) road. Black lines in (c)-(d) show the averaged mole fractions computed from these multiple transects. . 23
S1.21(a) CH_4mole fraction time series from the mobile near-surface measurements and (b) wind rose on **December 01, 2020**. Enhancement of CH_4mole fractions above the background in plume transects (c) & (d) along the near-landfill (ABC) road and (e) & (f) far-landfill remote road (EF). The distances along road segments are computed from A and E respectively for near-landfill (ABC) and far-landfill (EF) roads. Black lines in (c)-(f) show the averaged mole fractions computed from these multiple transects. 24
S1.22(a) CH_4mole fraction time series from the mobile near-surface measurements and (b) wind rose on **December 08, 2020**. Enhancement of CH_4mole fractions above the background in plume transects (c) & (d) along the near-landfill (ABC) road and (e) & (f) far-landfill remote road (EF). The distances along road segments are computed from A and E respectively for near-landfill (ABC) and far-landfill (EF) roads. Black lines in (c)-(f) show the averaged mole fractions computed from these multiple transects. 25

Figure S1.1. The development of the Butte-Bellot landfill as depicted in satellite imagery provided by Google Earth (©Google Earth). The years that each image was captured, progressing from left to right in each row, and from the top row to the bottom row, are: 2003, 2005, 2007, 2009, 2014, 2015, 2016, 2018, and 2020. These images suggest that the Eastern side of the landfill has been filled sequentially in three cells starting in the North-East (active 2005,2007) then progressing to the East (active: 2014, 2015) and finally the South-East (active since 2018 to 2020).

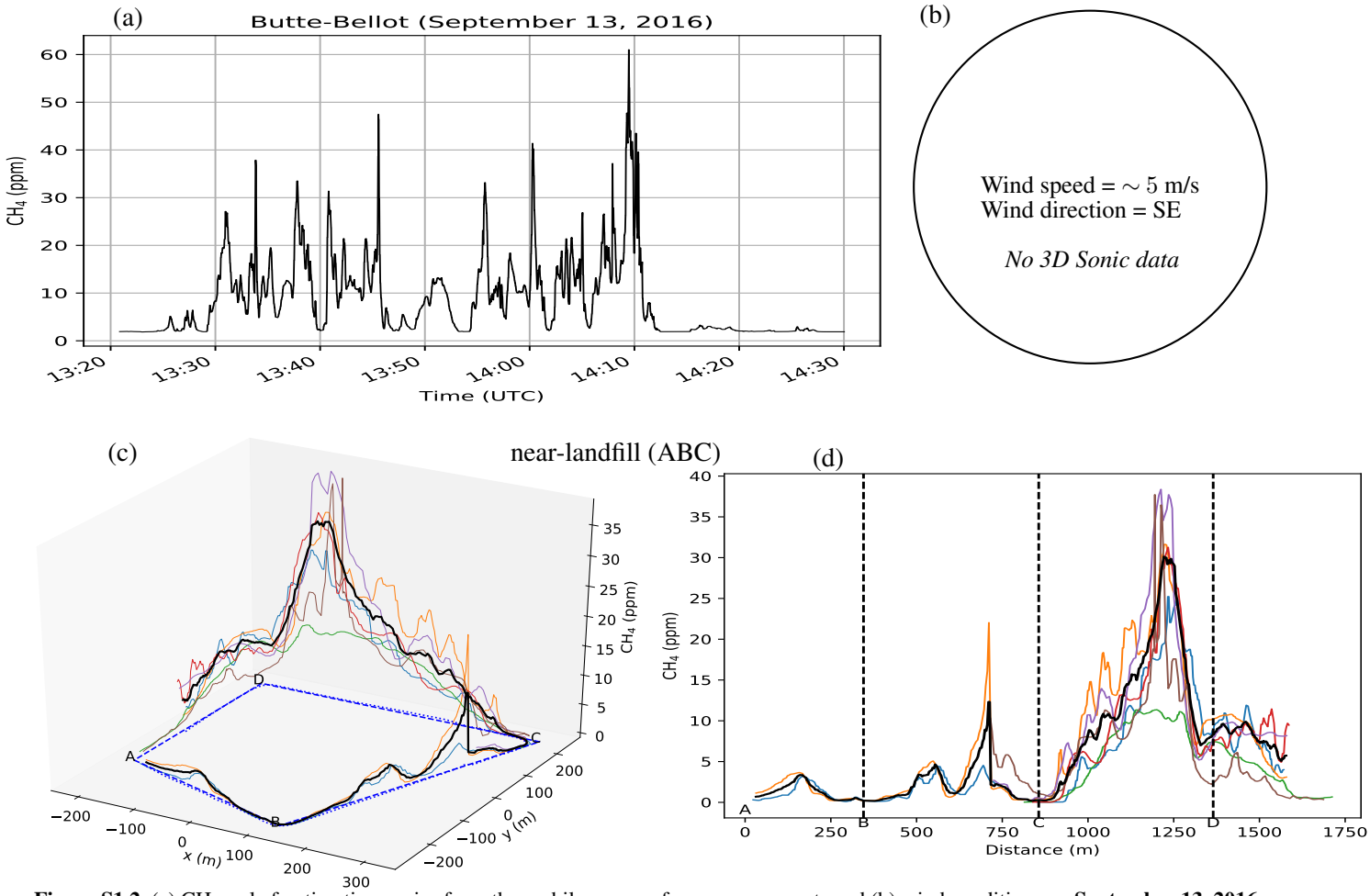

Figure S1.2. (a) CH_4mole fraction time series from the mobile near-surface measurements and (b) wind conditions on **September 13, 2016**. Enhancement of CH_4mole fractions above the background in plume transects (c) & (d) along the near-landfill (ABCD) road. The distances along road segments are computed from A towards anticlockwise direction . Black lines in (c)-(d) show the averaged mole fractions computed from these multiple transects.

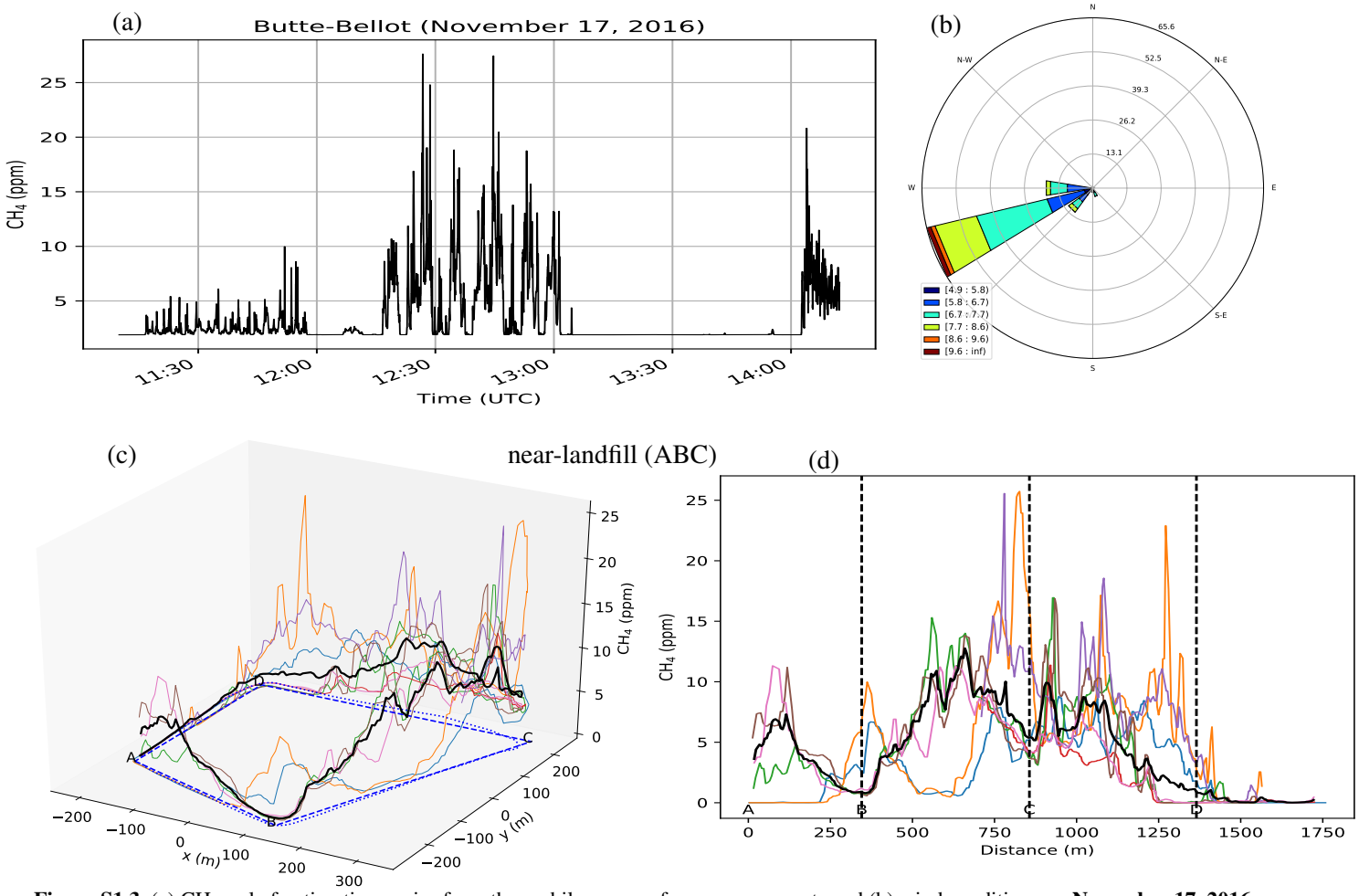

Figure S1.3. (a) CH_4mole fraction time series from the mobile near-surface measurements and (b) wind conditions on **November 17, 2016**. Enhancement of CH_4mole fractions above the background in plume transects (c) & (d) along the near-landfill (ABCD) road. The distances along road segments are computed from A towards anticlockwise direction . Black lines in (c)-(d) show the averaged mole fractions computed from these multiple transects.

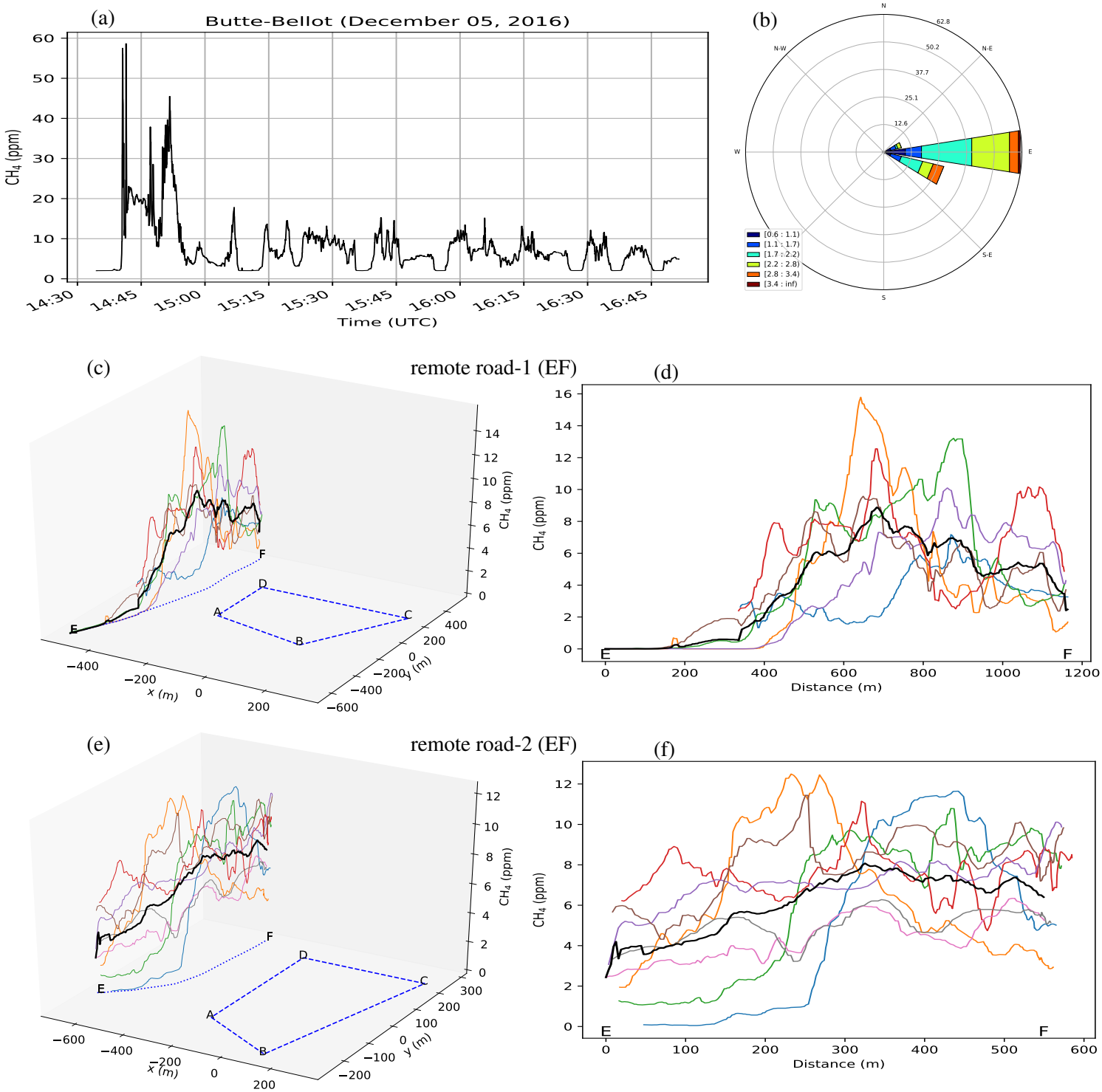

Figure S1.4. (a) CH_4mole fraction time series from the mobile near-surface measurements and (b) wind rose on **December 05, 2016**. Enhancement of CH_4mole fractions above the background in plume transects along the first (c) & (d) and the second (e) & (f) remote roads. The distances along road segments are computed from E . Black lines in (c)-(f) show the averaged mole fractions computed from these multiple transects.

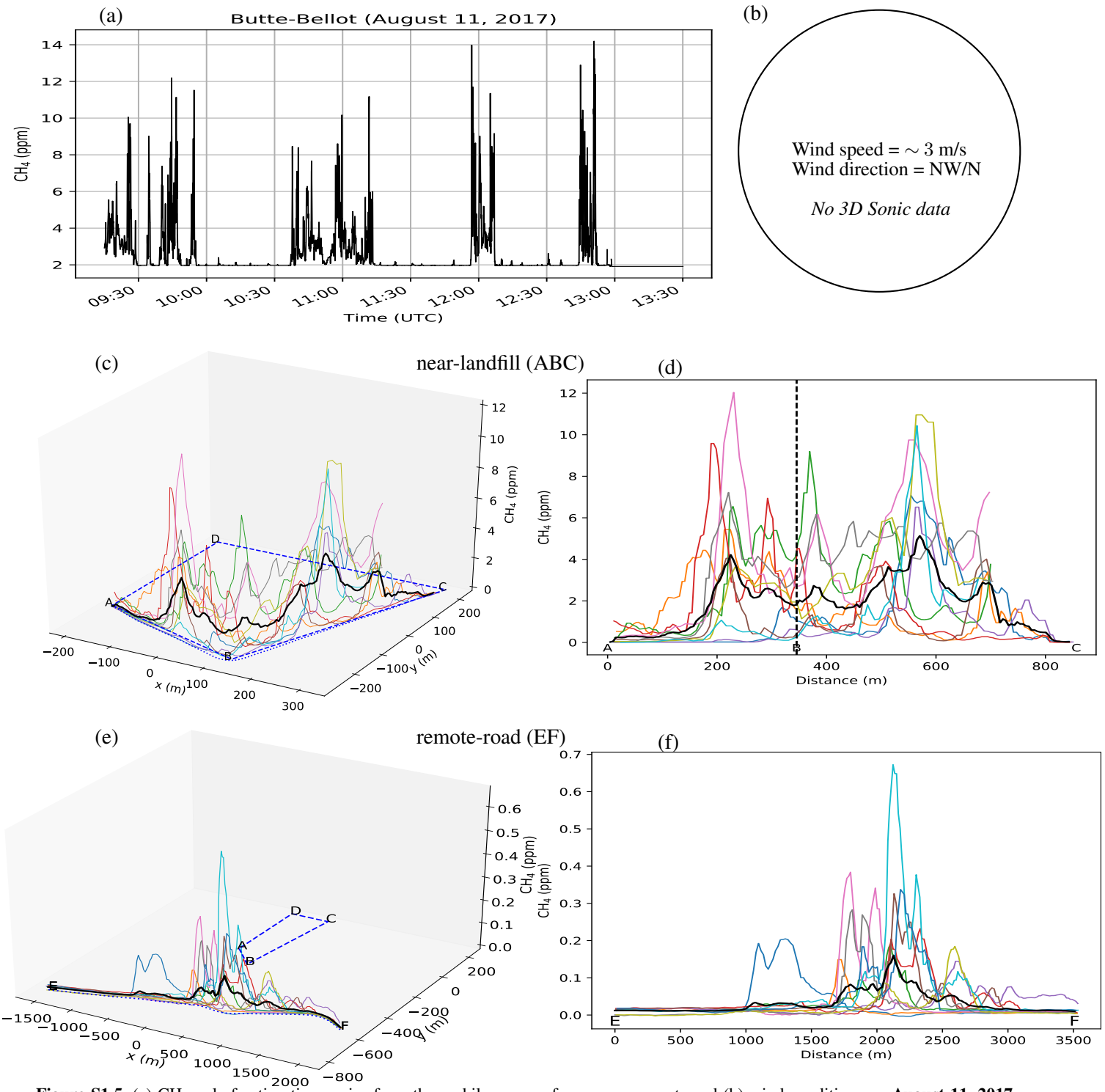

Figure S1.5. (a) CH_4mole fraction time series from the mobile near-surface measurements and (b) wind conditions on **August 11, 2017**. Enhancement of CH_4mole fractions above the background in plume transects (c) & (d) along the near-landfill (ABC) road and (e) & (f) far-landfill remote road (EF). The distances along road segments are computed from A and E respectively for near-landfill (ABC) and far-landfill (EF) roads. Black lines in (c)-(f) show the averaged mole fractions computed from these multiple transects.

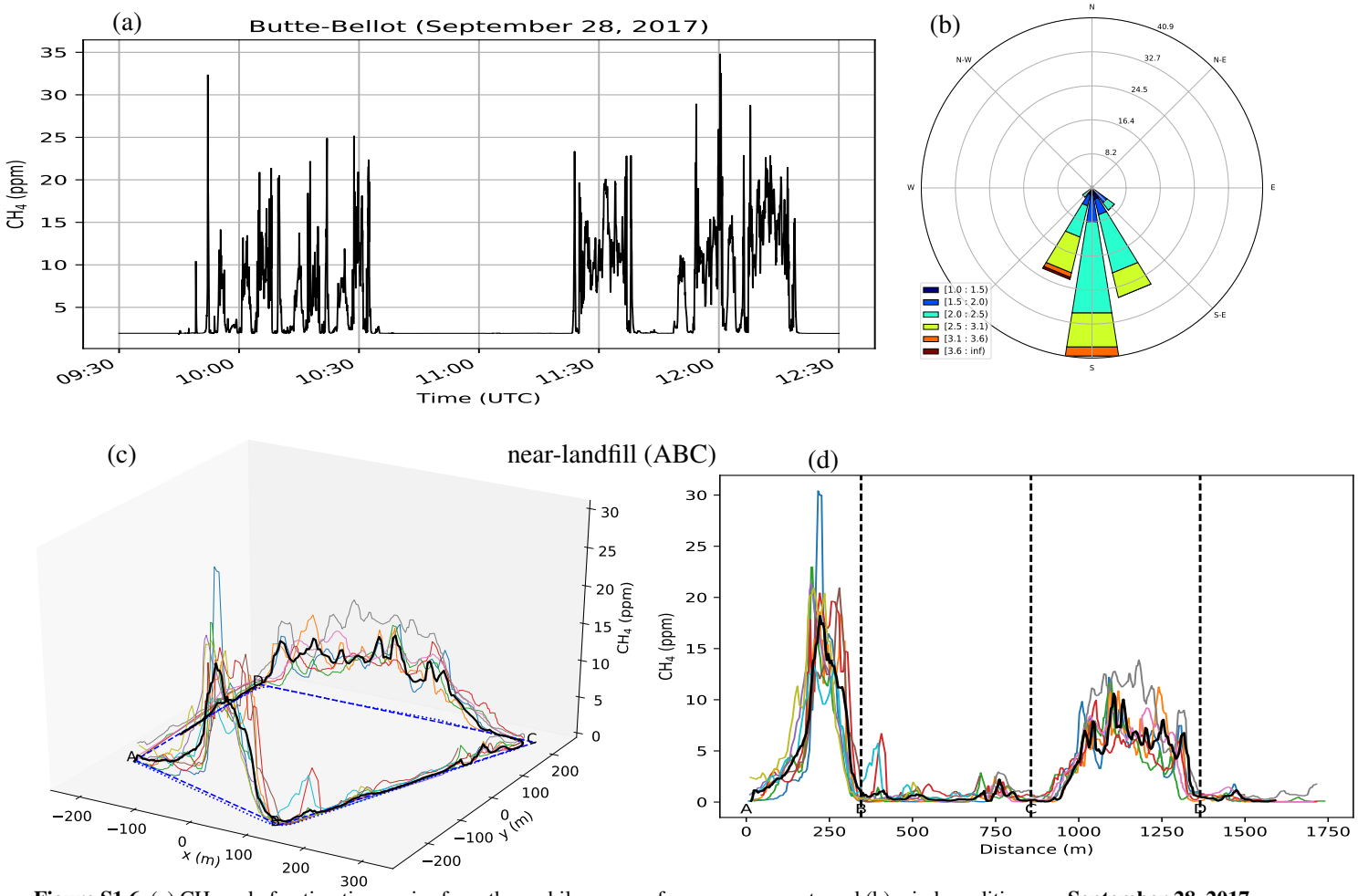

Figure S1.6. (a) CH_4mole fraction time series from the mobile near-surface measurements and (b) wind conditions on **September 28, 2017**. Enhancement of CH_4mole fractions above the background in plume transects (c) & (d) along the near-landfill (ABC) road. The distances along road segments are computed from A towards anticlockwise direction. Black lines in (c)-(d) show the averaged mole fractions computed from these multiple transects.

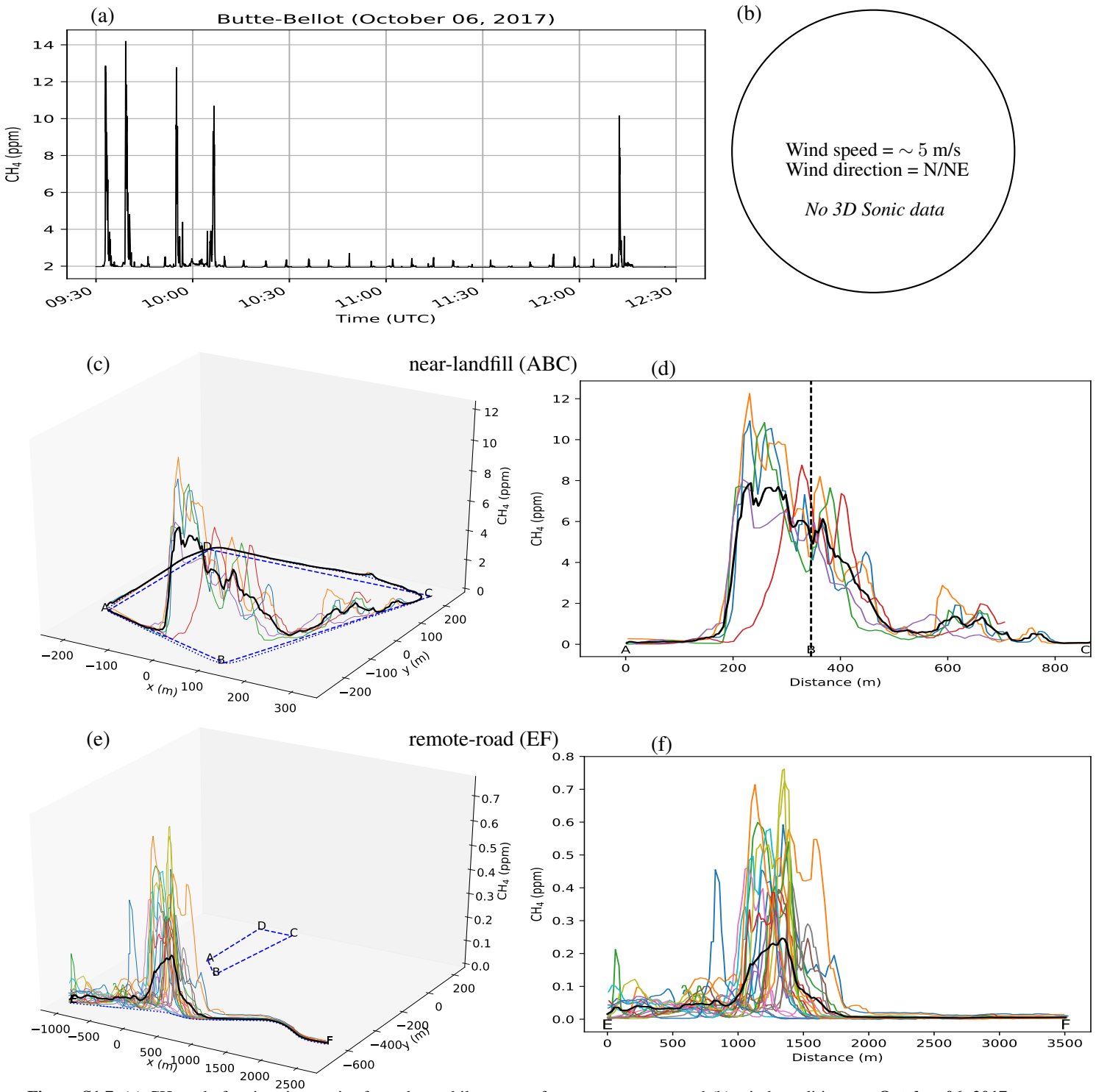

Figure S1.7. (a) CH_4mole fraction time series from the mobile near-surface measurements and (b) wind conditions on **October 06, 2017**. Enhancement of CH_4mole fractions above the background in plume transects (c) & (d) along the near-landfill (ABC) road and (e) & (f) far-landfill remote road (EF). The distances along road segments are computed from A and E respectively for near-landfill (ABC) and far-landfill (EF) roads. Black lines in (c)-(f) show the averaged mole fractions computed from these multiple transects.

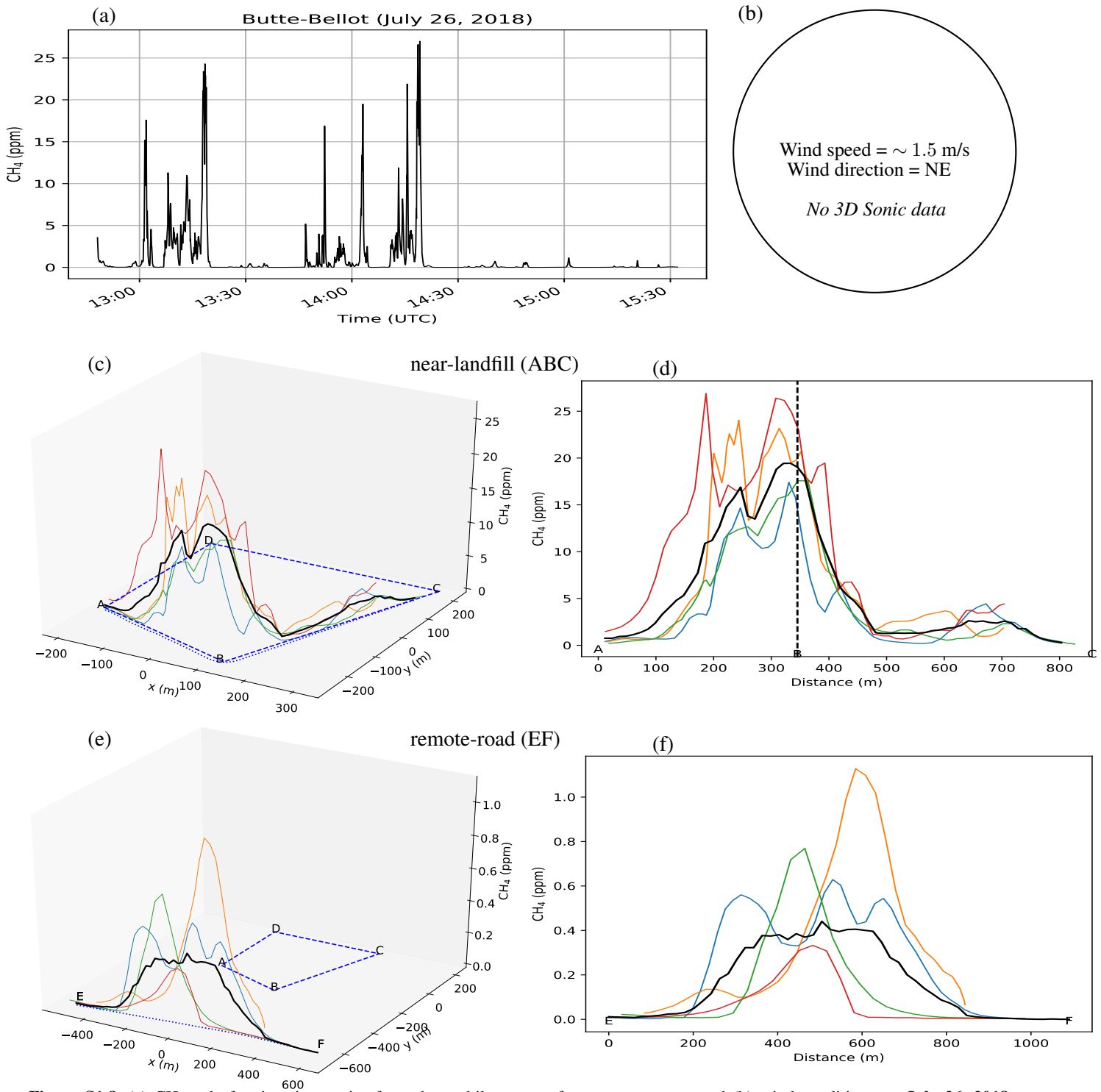

Figure S1.8. (a) CH_4mole fraction time series from the mobile near-surface measurements and (b) wind conditions on **July 26, 2018**. Enhancement of CH_4mole fractions above the background in plume transects (c) & (d) along the near-landfill (ABC) road and (e) & (f) far-landfill remote road (EF). The distances along road segments are computed from A and E respectively for near-landfill (ABC) and far-landfill (EF) roads. Black lines in (c)-(f) show the averaged mole fractions computed from these multiple transects.

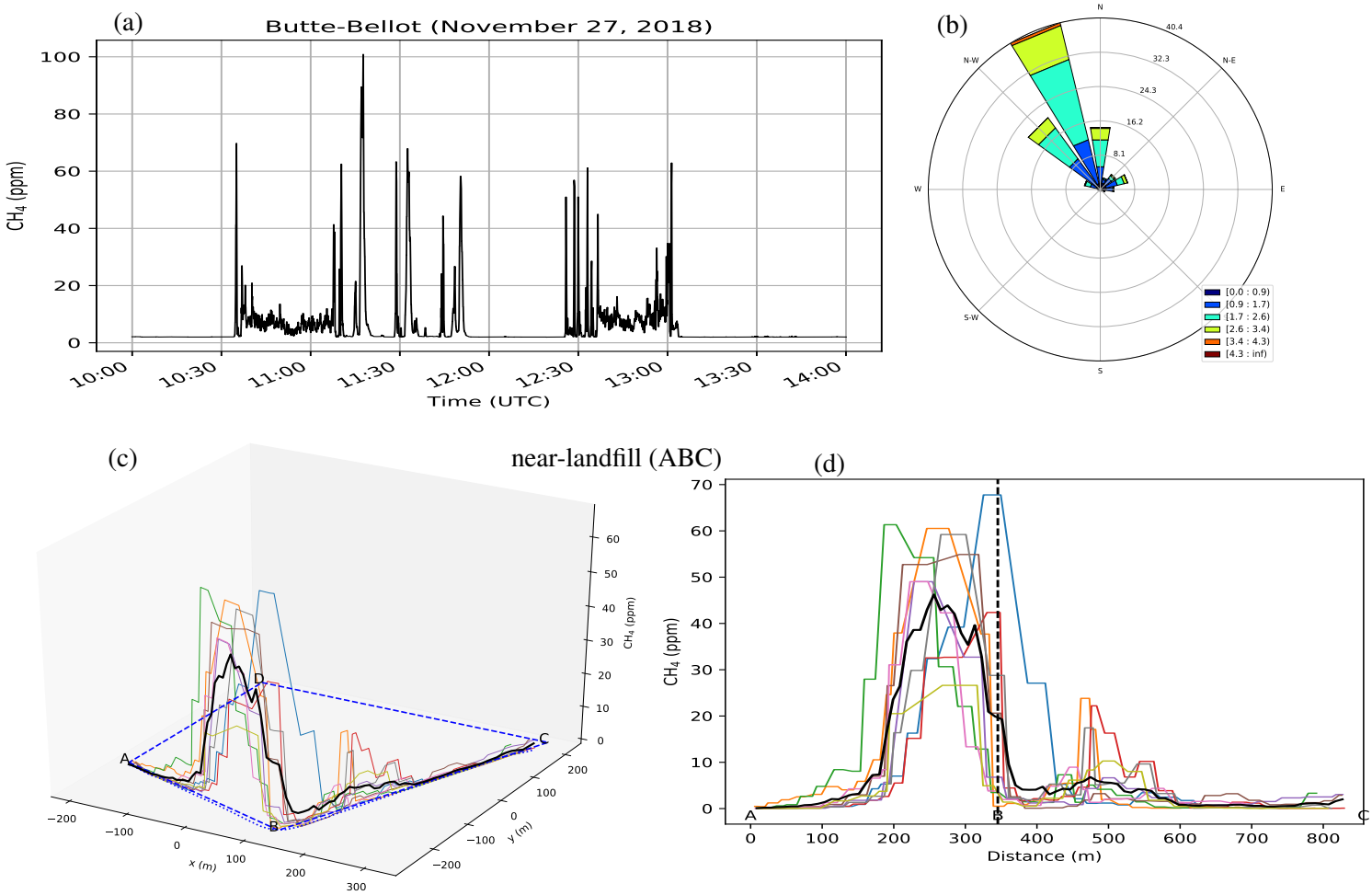

Figure S1.9. (a) CH_4mole fraction time series from the mobile near-surface measurements and (b) wind rose on **November 27, 2018**. Enhancement of CH_4mole fractions above the background in plume transects (c) & (d) along the near-landfill (ABC) road. The distances along road segments are computed from A. Black lines in (c)-(d) show the averaged mole fractions computed from these multiple transects.

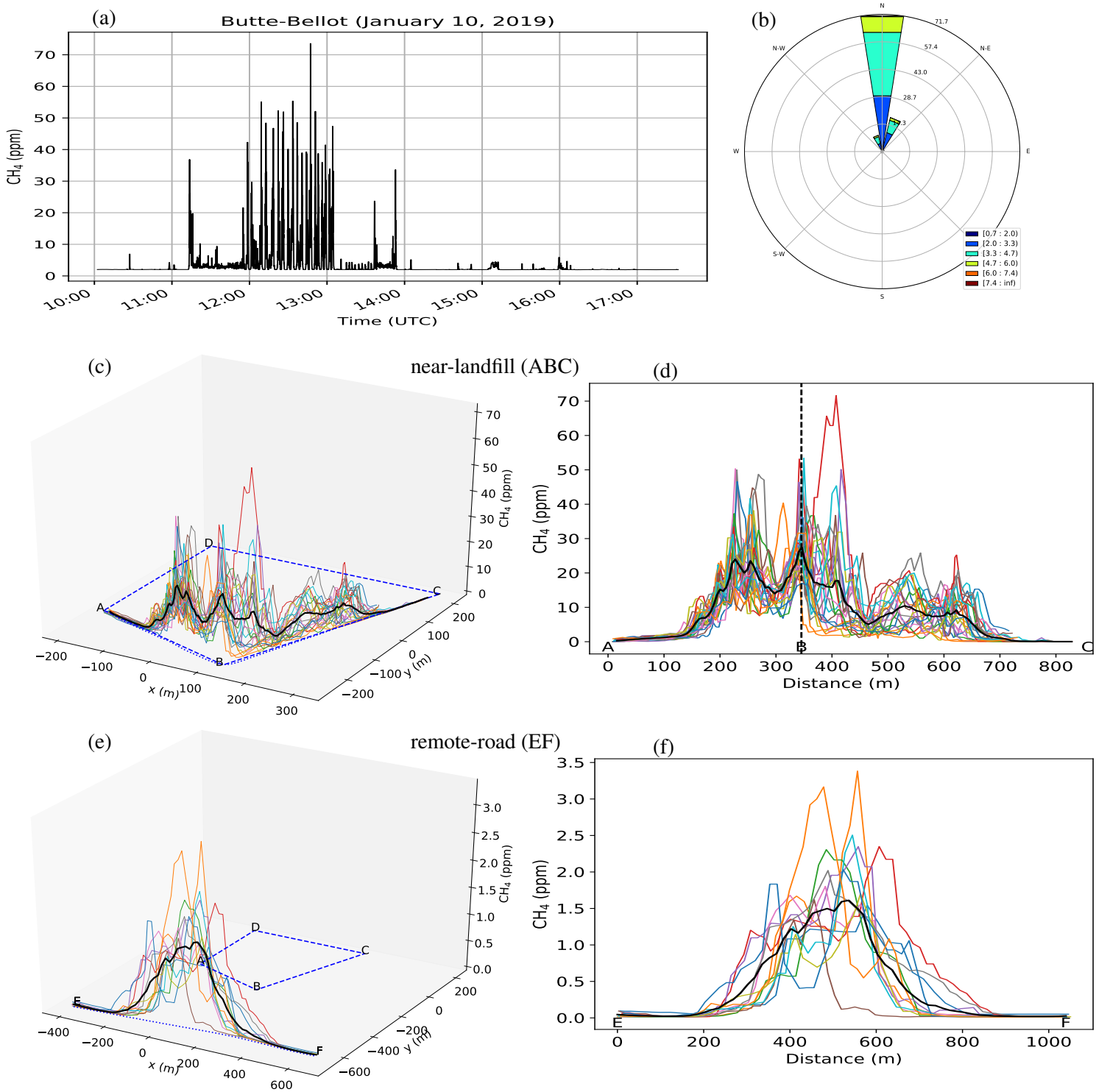

Figure S1.10. (a) CH_4mole fraction time series from the mobile near-surface measurements and (b) wind rose on **January 10, 2019**. Enhancement of CH_4mole fractions above the background in plume transects (c) & (d) along the near-landfill (ABC) road and (e) & (f) far-landfill remote road (EF). The distances along road segments are computed from A and E respectively for near-landfill (ABC) and far-landfill (EF) roads. Black lines in (c)-(f) show the averaged mole fractions computed from these multiple transects.

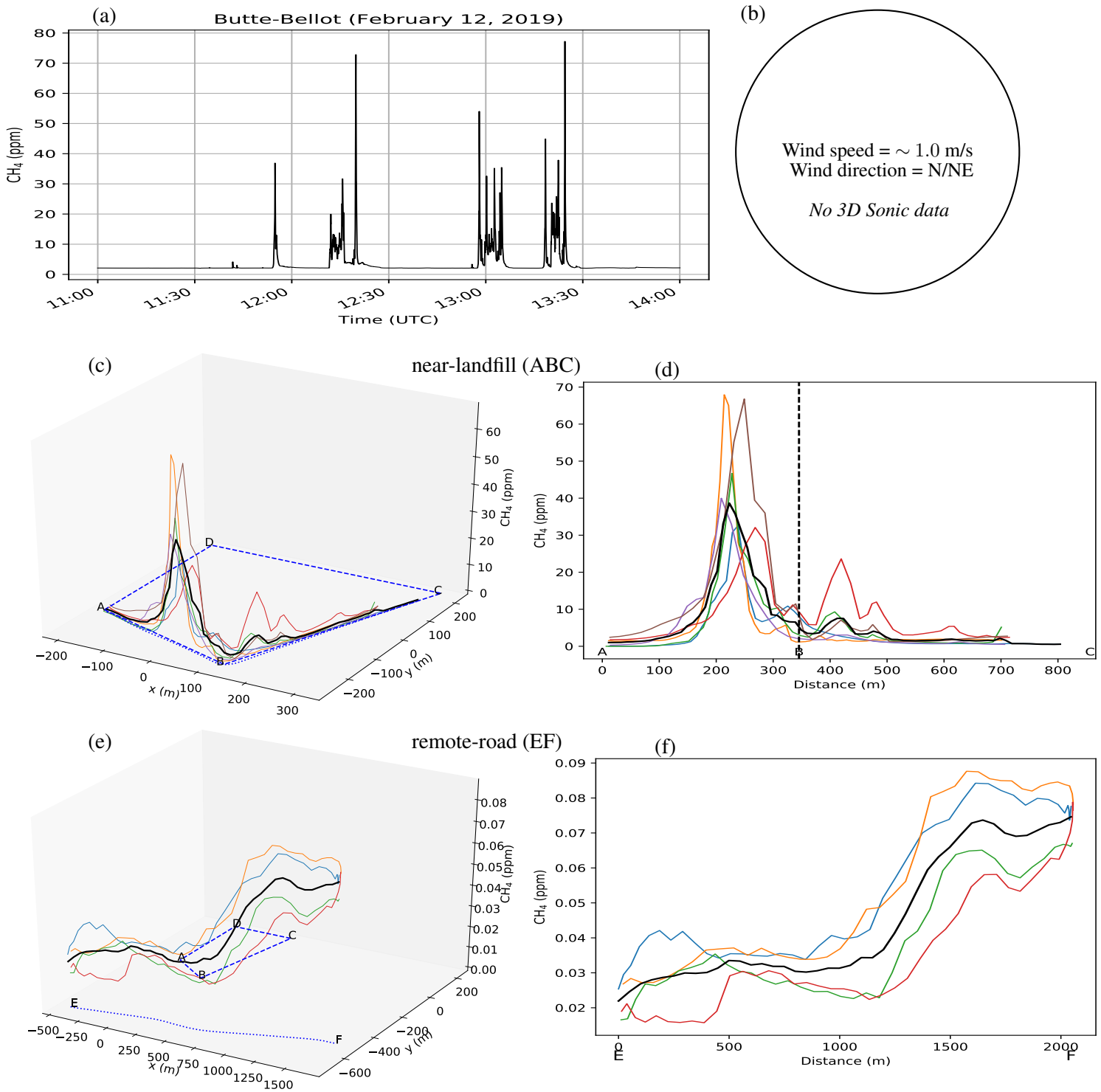

Figure S1.11. (a) CH_4 mole fraction time series from the mobile near-surface measurements and (b) wind conditions on **February 12, 2019**. Enhancement of CH_4 mole fractions above the background in plume transects (c) & (d) along the near-landfill (ABC) road and (e) & (f) far-landfill remote road (EF). The distances along road segments are computed from A and E respectively for near-landfill (ABC) and far-landfill (EF) roads. Black lines in (c)-(f) show the averaged mole fractions computed from these multiple transects.

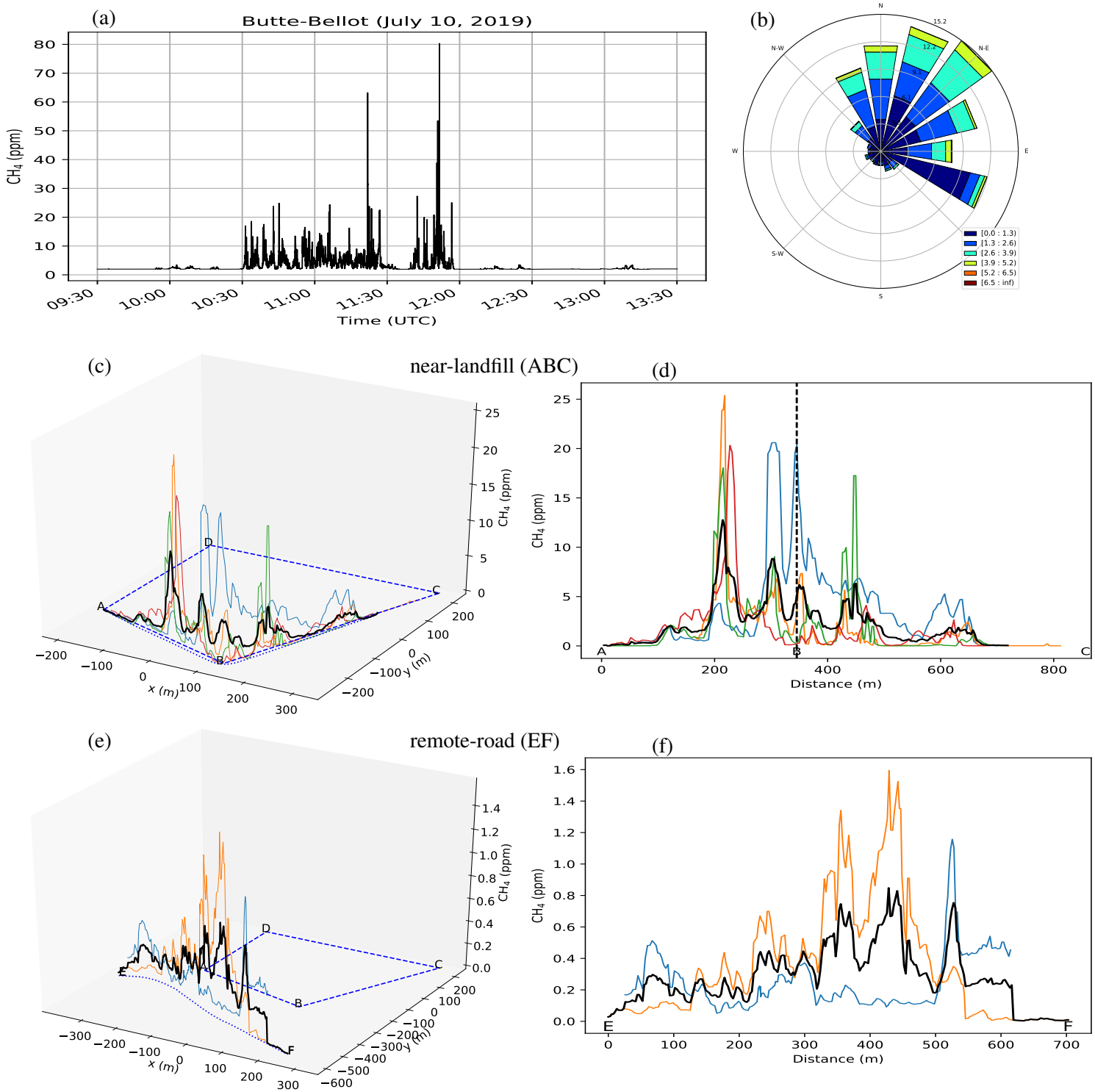

Figure S1.12. (a) CH_4mole fraction time series from the mobile near-surface measurements and (b) wind rose on **July 10, 2019**. Enhancement of CH_4mole fractions above the background in plume transects (c) & (d) along the near-landfill (ABC) road and (e) & (f) far-landfill remote road (EF). The distances along road segments are computed from A and E respectively for near-landfill (ABC) and far-landfill (EF) roads. Black lines in (c)-(f) show the averaged mole fractions computed from these multiple transects.

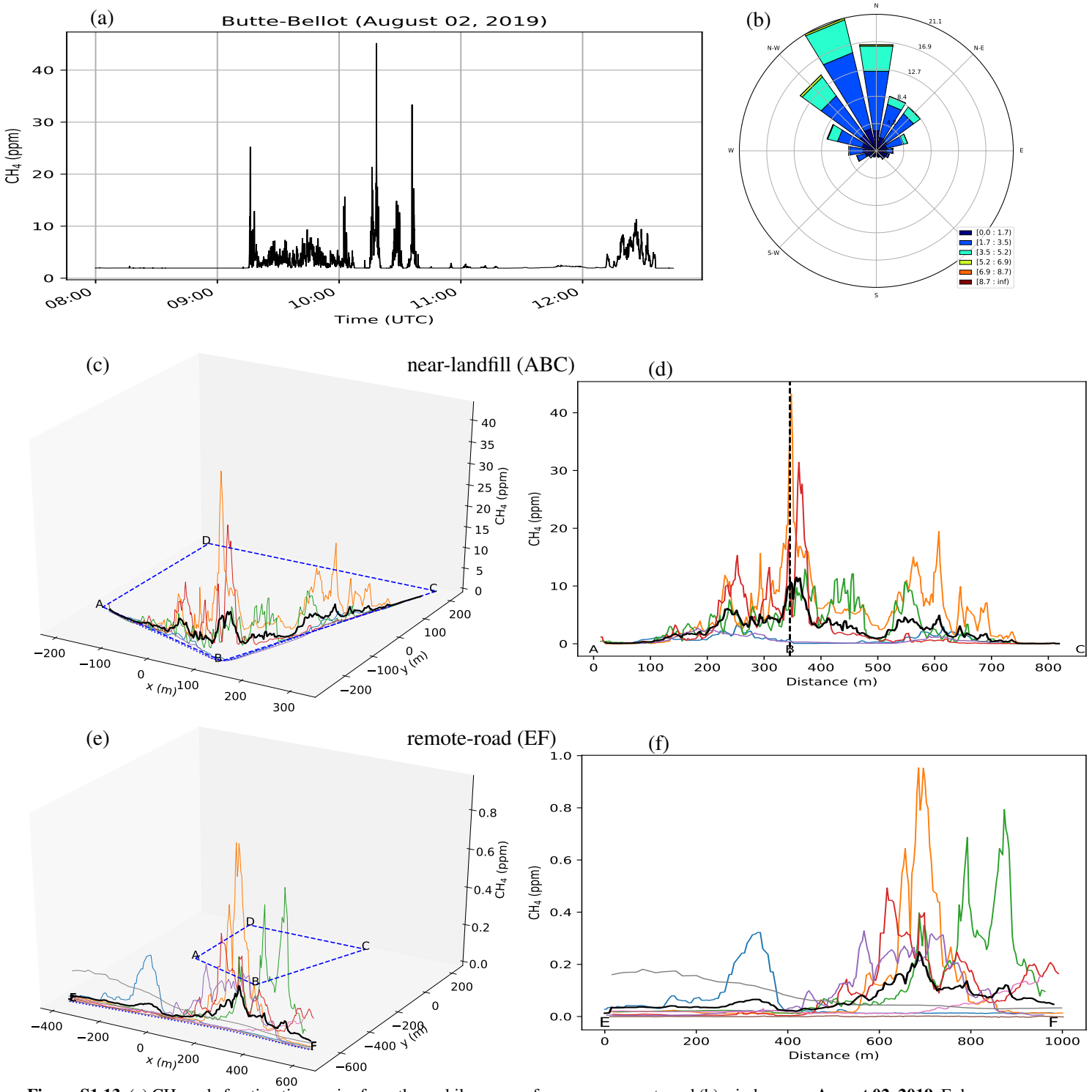

Figure S1.13. (a) CH_4mole fraction time series from the mobile near-surface measurements and (b) wind rose on **August 02, 2019**. Enhancement of CH_4mole fractions above the background in plume transects (c) & (d) along the near-landfill (ABC) road and (e) & (f) far-landfill remote road (EF). The distances along road segments are computed from A and E respectively for near-landfill (ABC) and far-landfill (EF) roads. Black lines in (c)-(f) show the averaged mole fractions computed from these multiple transects.

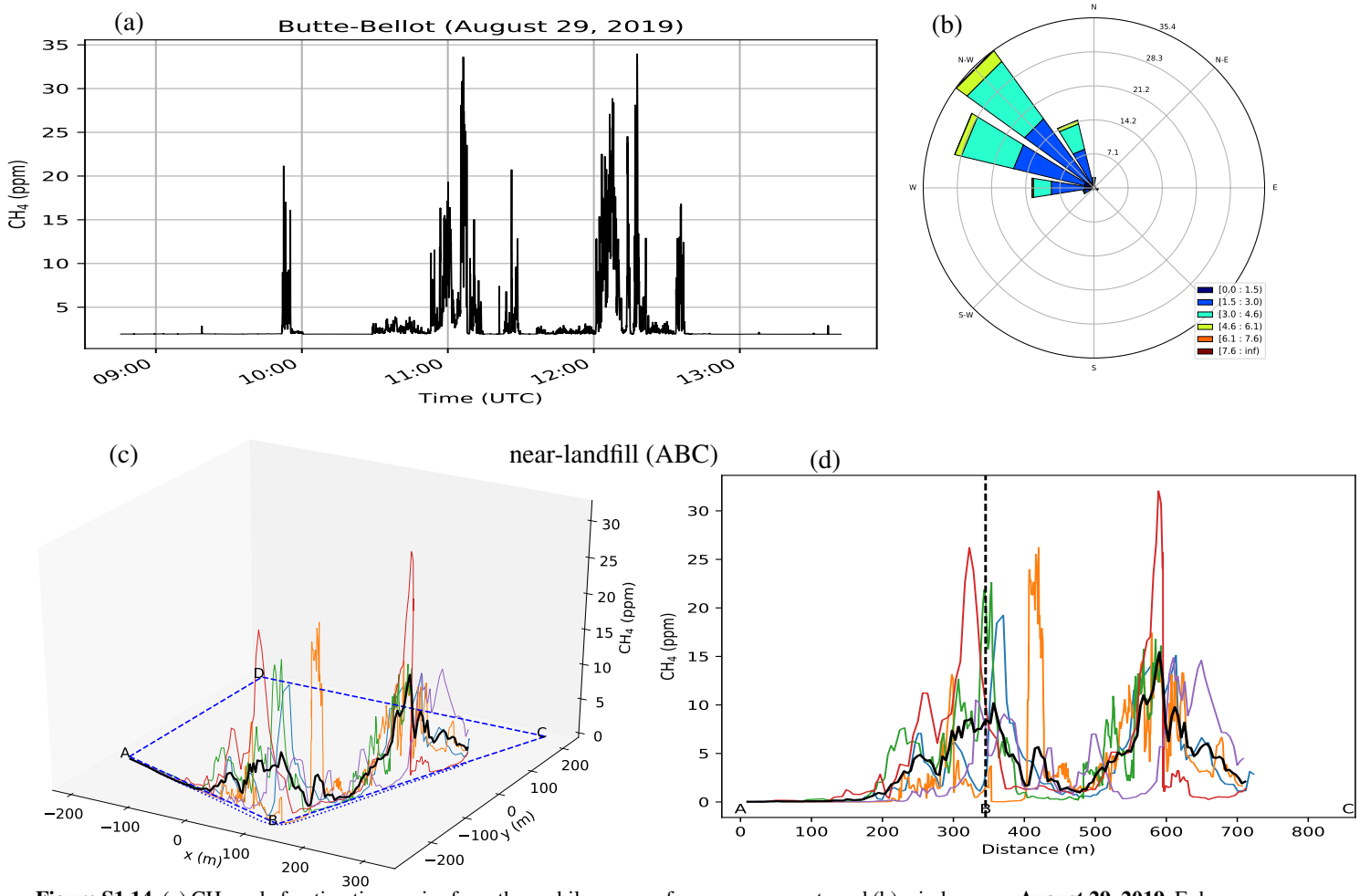

Figure S1.14. (a) CH_4mole fraction time series from the mobile near-surface measurements and (b) wind rose on **August 29, 2019**. Enhancement of CH_4mole fractions above the background in plume transects (c) & (d) along the near-landfill (ABC) road. The distances along road segments are computed from A. Black lines in (c)-(d) show the averaged mole fractions computed from these multiple transects.

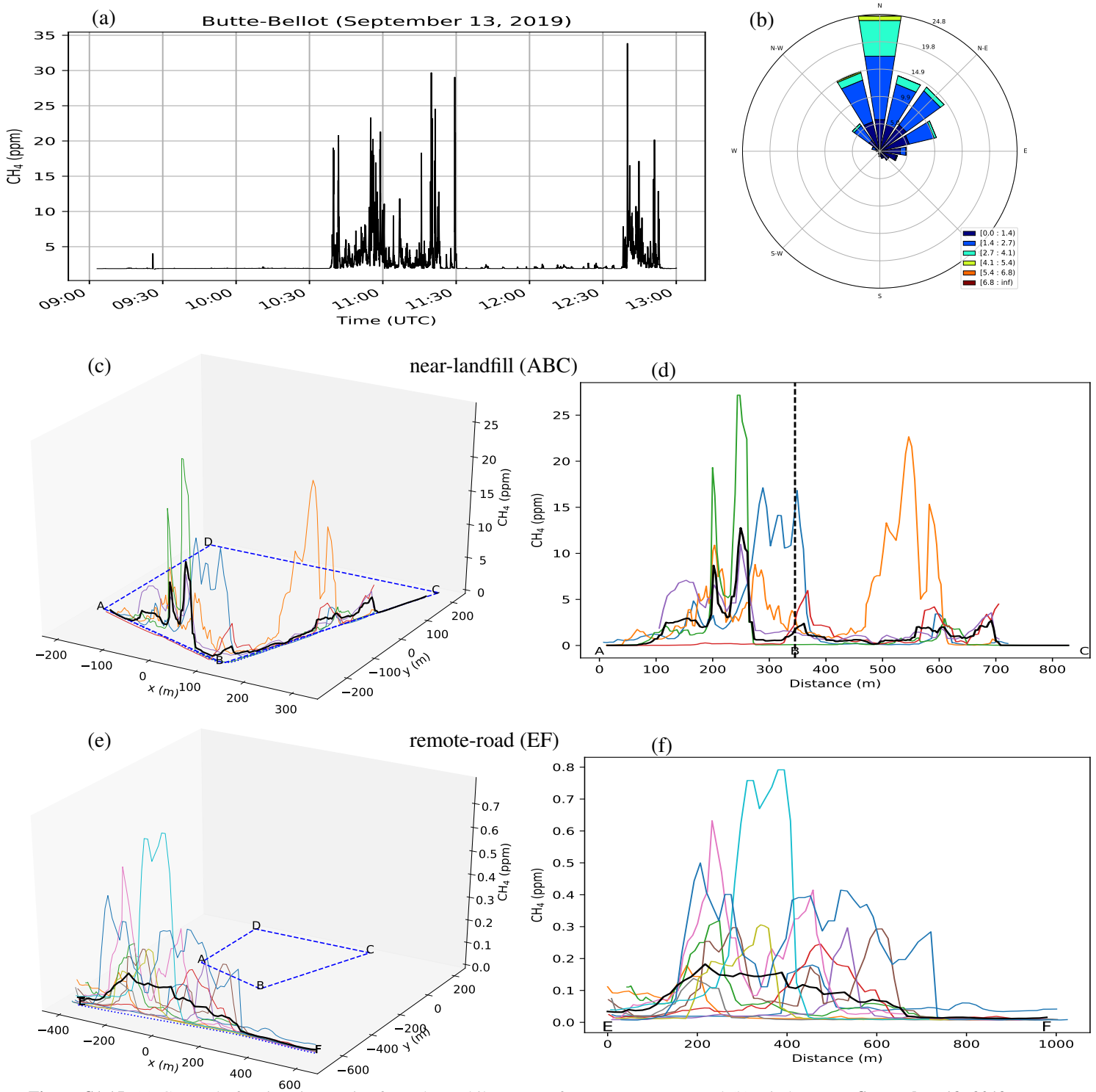

Figure S1.15. (a) CH_4mole fraction time series from the mobile near-surface measurements and (b) wind rose on **September 13, 2019**. Enhancement of CH_4mole fractions above the background in plume transects (c) & (d) along the near-landfill (ABC) road and (e) & (f) far-landfill remote road (EF). The distances along road segments are computed from A and E respectively for near-landfill (ABC) and far-landfill (EF) roads. Black lines in (c)-(f) show the averaged mole fractions computed from these multiple transects.

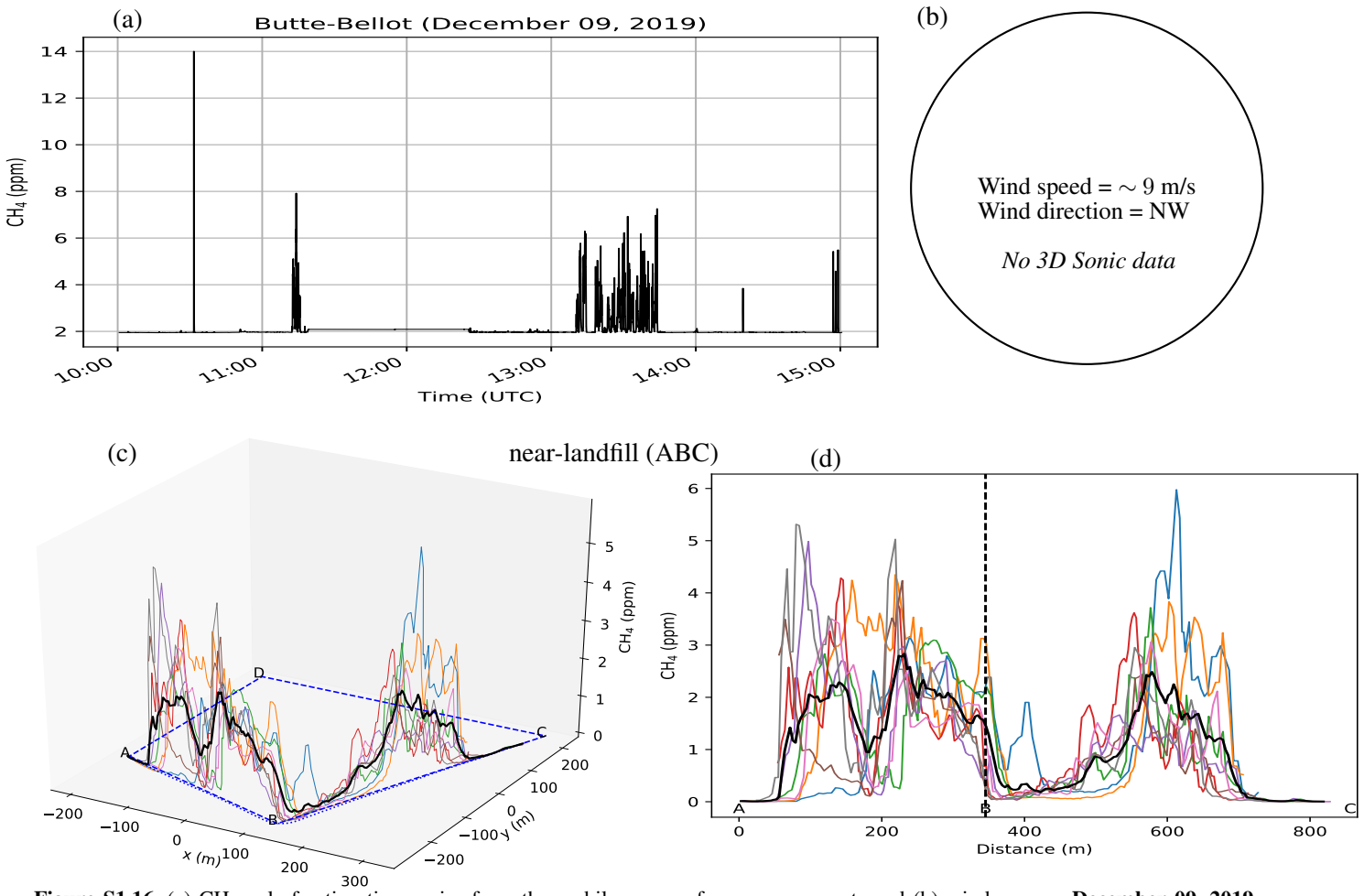

Figure S1.16. (a) CH_4mole fraction time series from the mobile near-surface measurements and (b) wind rose on **December 09, 2019**. Enhancement of CH_4mole fractions above the background in plume transects (c) & (d) along the near-landfill (ABC) road and (e) & (f) far-landfill remote road (EF). The distances along road segments are computed from A and E respectively for near-landfill (ABC) and far-landfill (EF) roads. Black lines in (c)-(f) show the averaged mole fractions computed from these multiple transects.

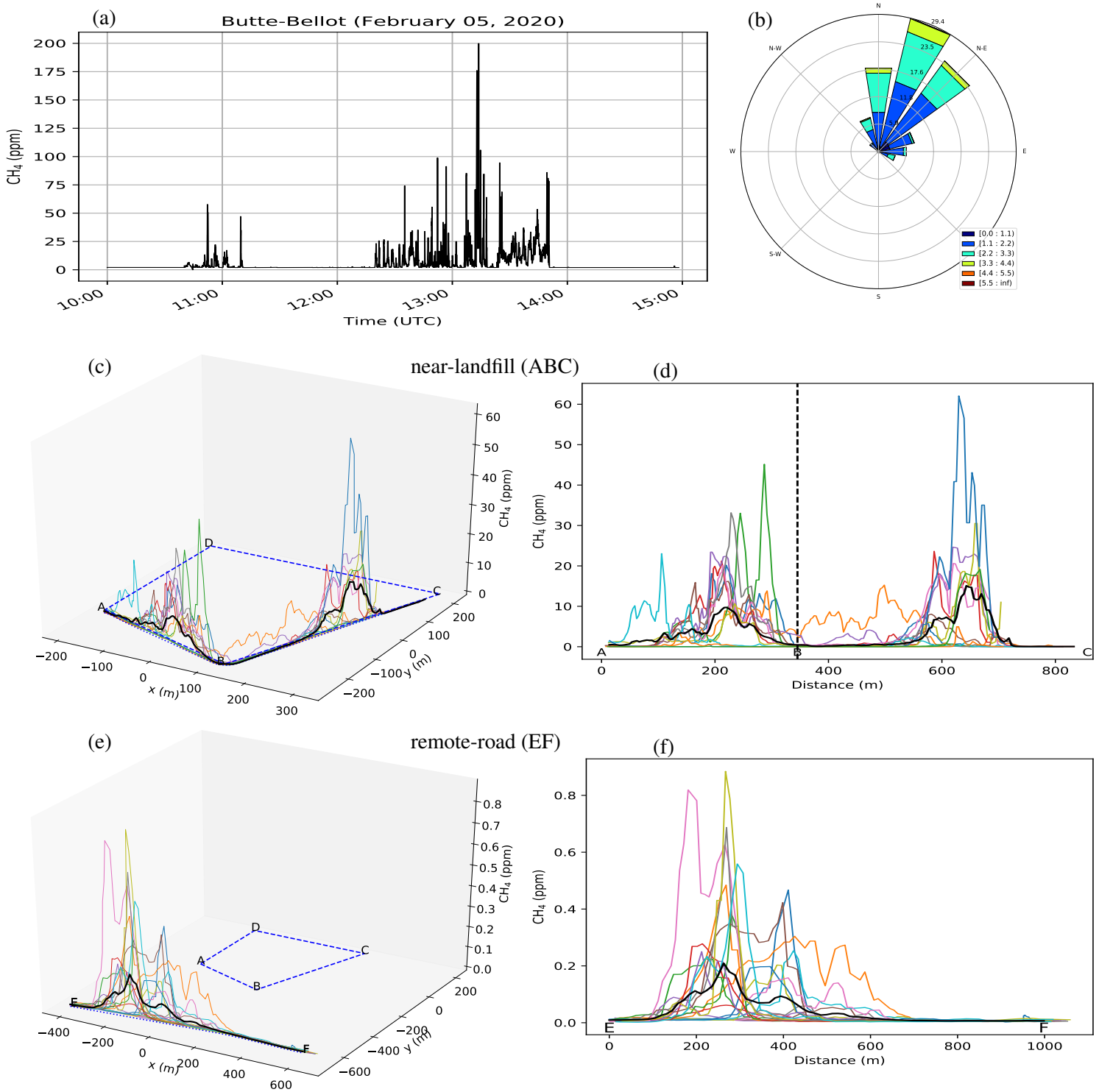

Figure S1.17. (a) CH_4mole fraction time series from the mobile near-surface measurements and (b) wind rose on **February 05, 2020**. Enhancement of CH_4mole fractions above the background in plume transects (c) & (d) along the near-landfill (ABC) road and (e) & (f) far-landfill remote road (EF). The distances along road segments are computed from A and E respectively for near-landfill (ABC) and far-landfill (EF) roads. Black lines in (c)-(f) show the averaged mole fractions computed from these multiple transects.

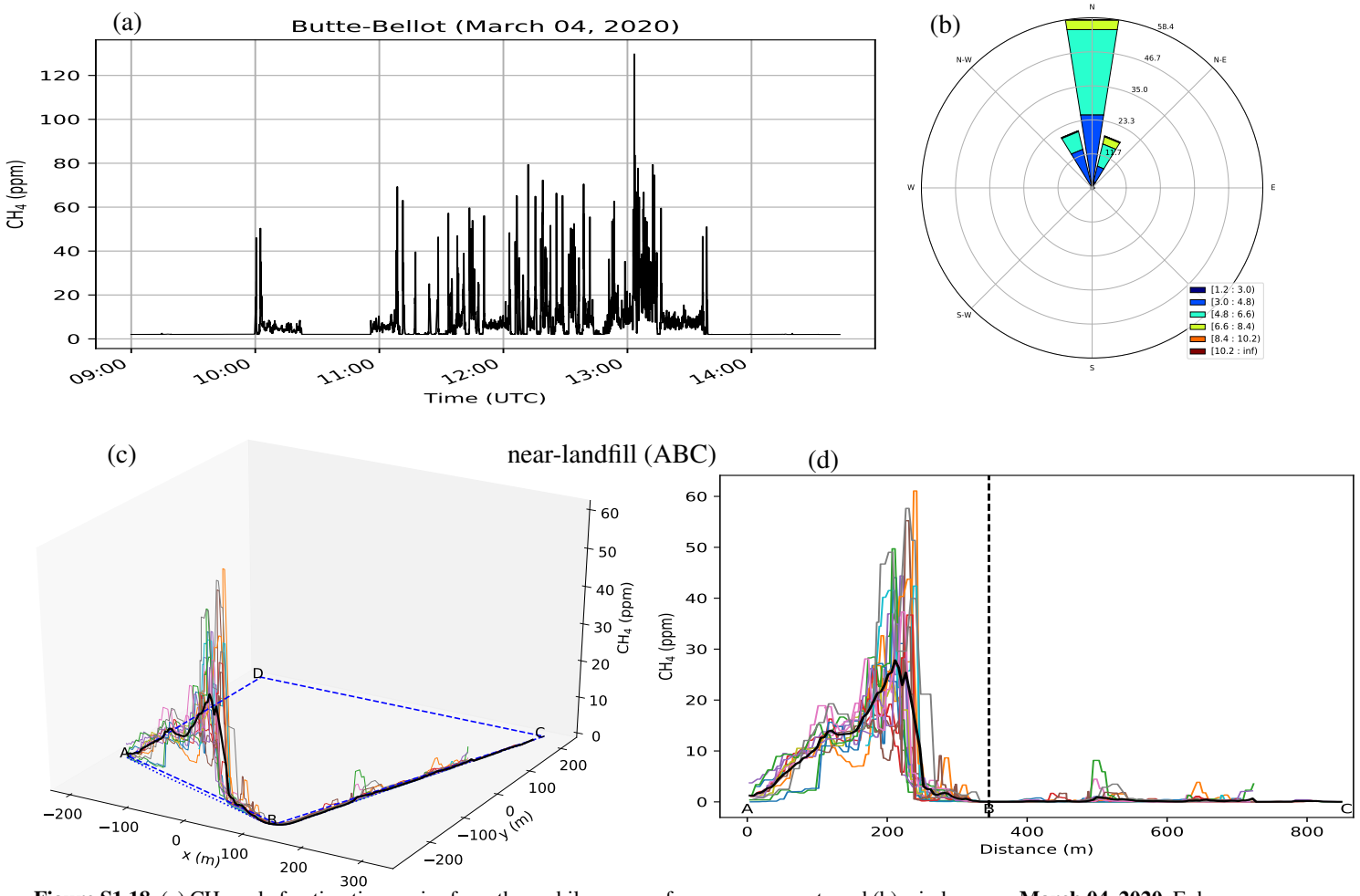

Figure S1.18. (a) CH_4 mole fraction time series from the mobile near-surface measurements and (b) wind rose on **March 04, 2020**. Enhancement of CH_4 mole fractions above the background in plume transects (c) & (d) along the near-landfill (ABC) road. The distances along road segments are computed from A for near-landfill (ABC) road. Black lines in (c)-(d) show the averaged mole fractions computed from these multiple transects.

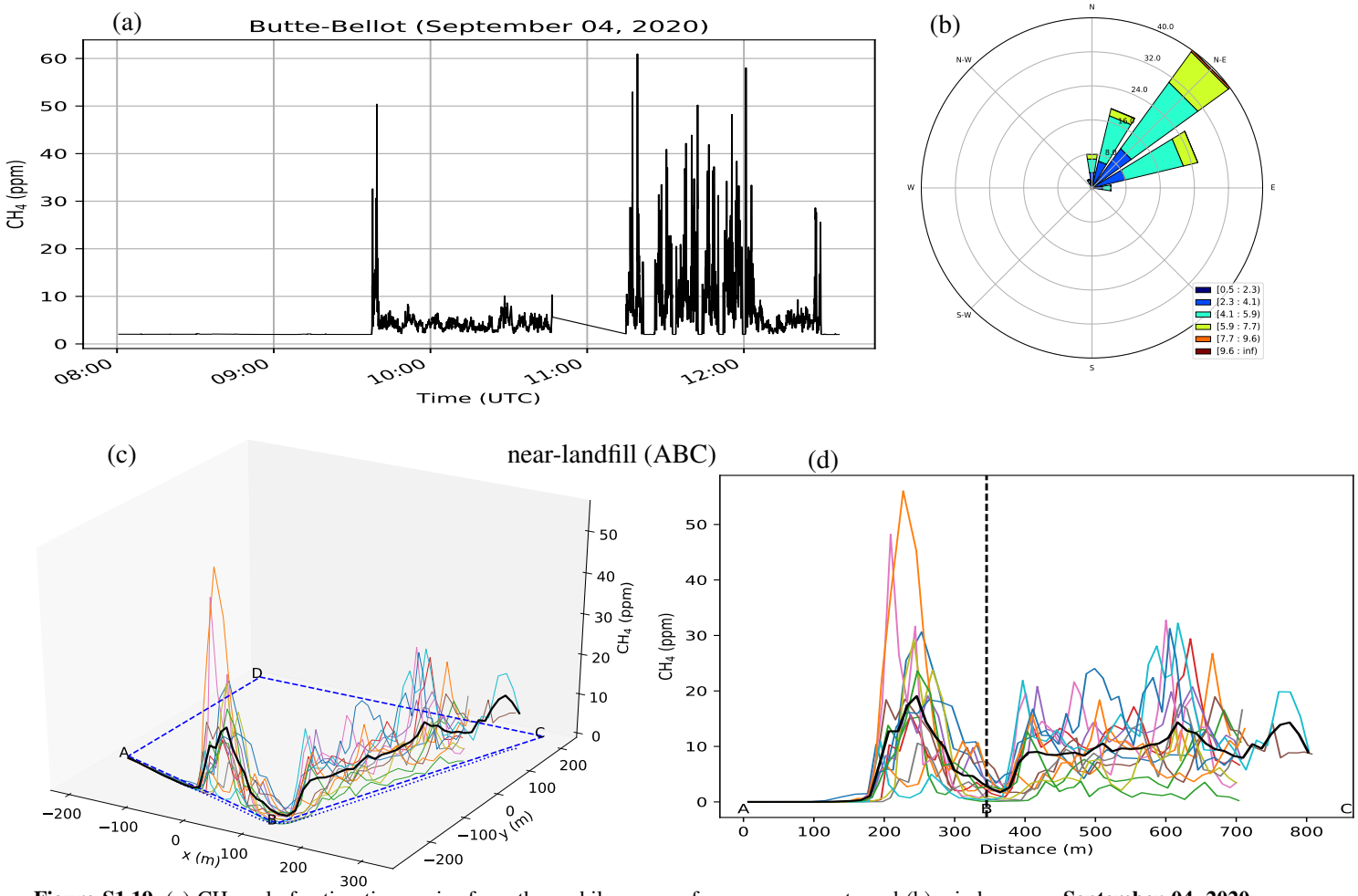

Figure S1.19. (a) CH_4mole fraction time series from the mobile near-surface measurements and (b) wind rose on **September 04, 2020**. Enhancement of CH_4mole fractions above the background in plume transects (c) & (d) along the near-landfill (ABC) road. The distances along road segments are computed from A for near-landfill (ABC) road. Black lines in (c)-(d) show the averaged mole fractions computed from these multiple transects.

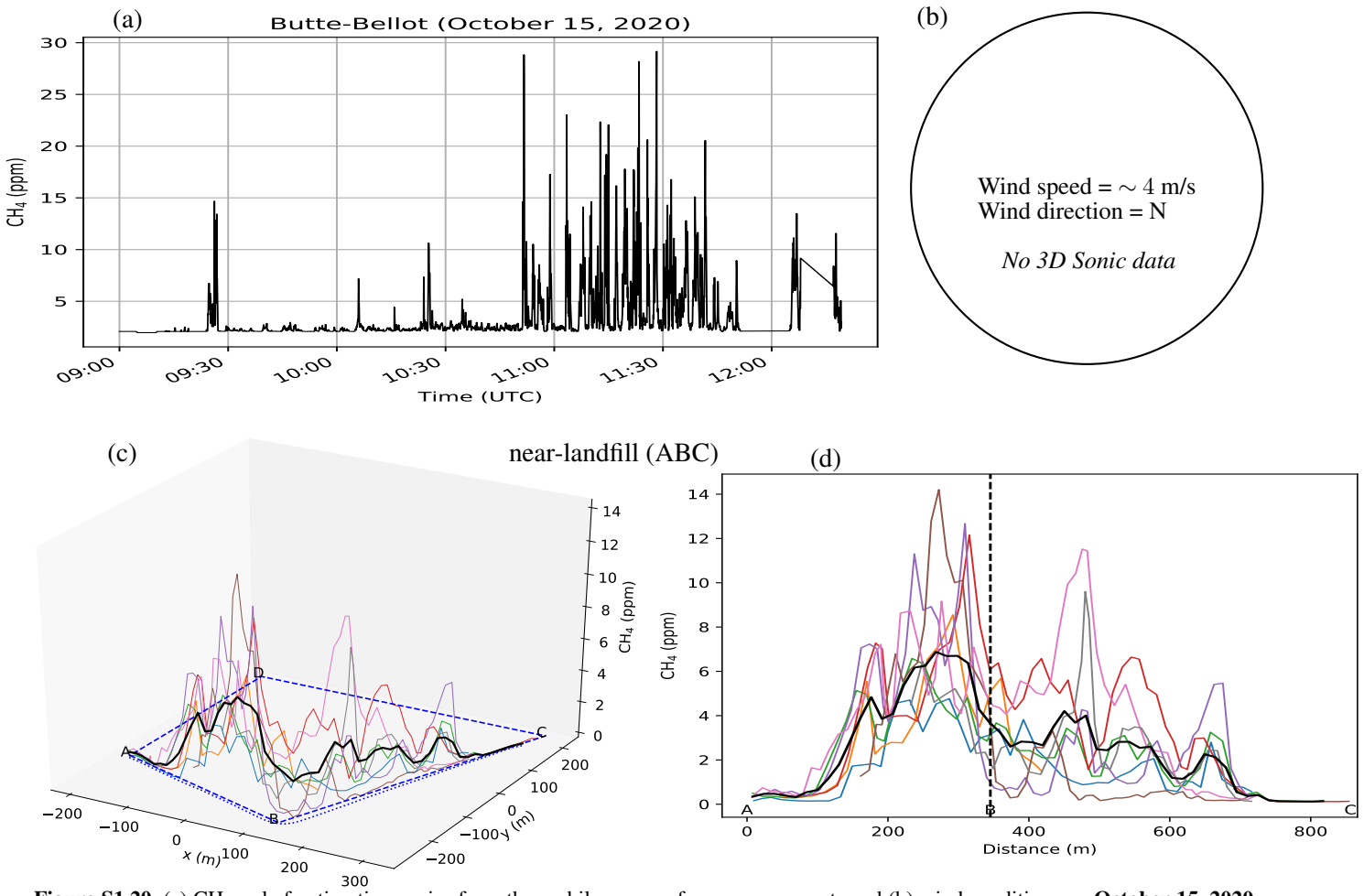

Figure S1.20. (a) CH_4mole fraction time series from the mobile near-surface measurements and (b) wind conditions on **October 15, 2020**. Enhancement of CH_4mole fractions above the background in plume transects (c) & (d) along the near-landfill (ABC) road. The distances along road segments are computed from A for near-landfill (ABC) road. Black lines in (c)-(d) show the averaged mole fractions computed from these multiple transects.

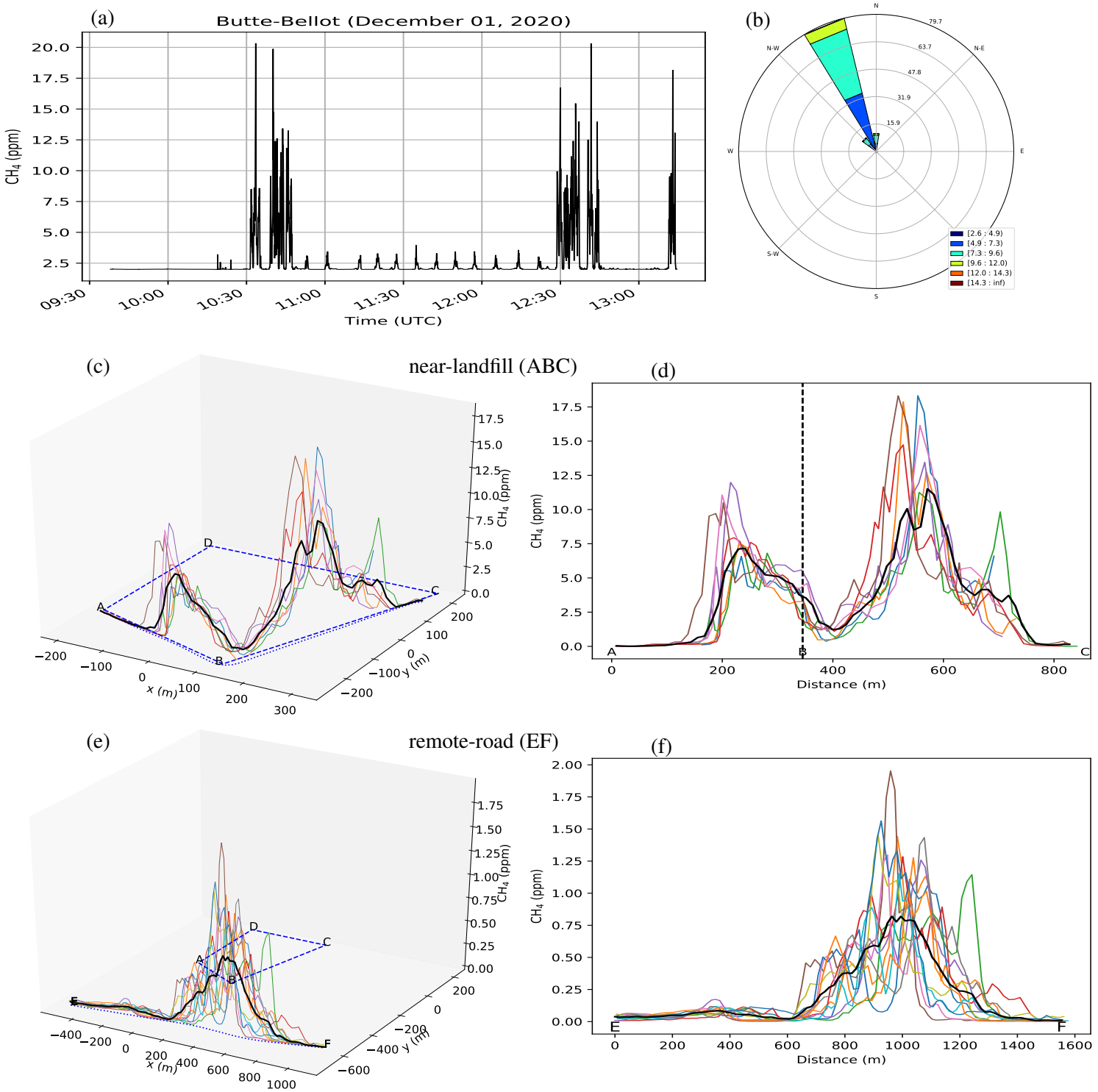

Figure S1.21. (a) CH_4mole fraction time series from the mobile near-surface measurements and (b) wind rose on **December 01, 2020**. Enhancement of CH_4mole fractions above the background in plume transects (c) & (d) along the near-landfill (ABC) road and (e) & (f) far-landfill remote road (EF). The distances along road segments are computed from A and E respectively for near-landfill (ABC) and far-landfill (EF) roads. Black lines in (c)-(f) show the averaged mole fractions computed from these multiple transects.

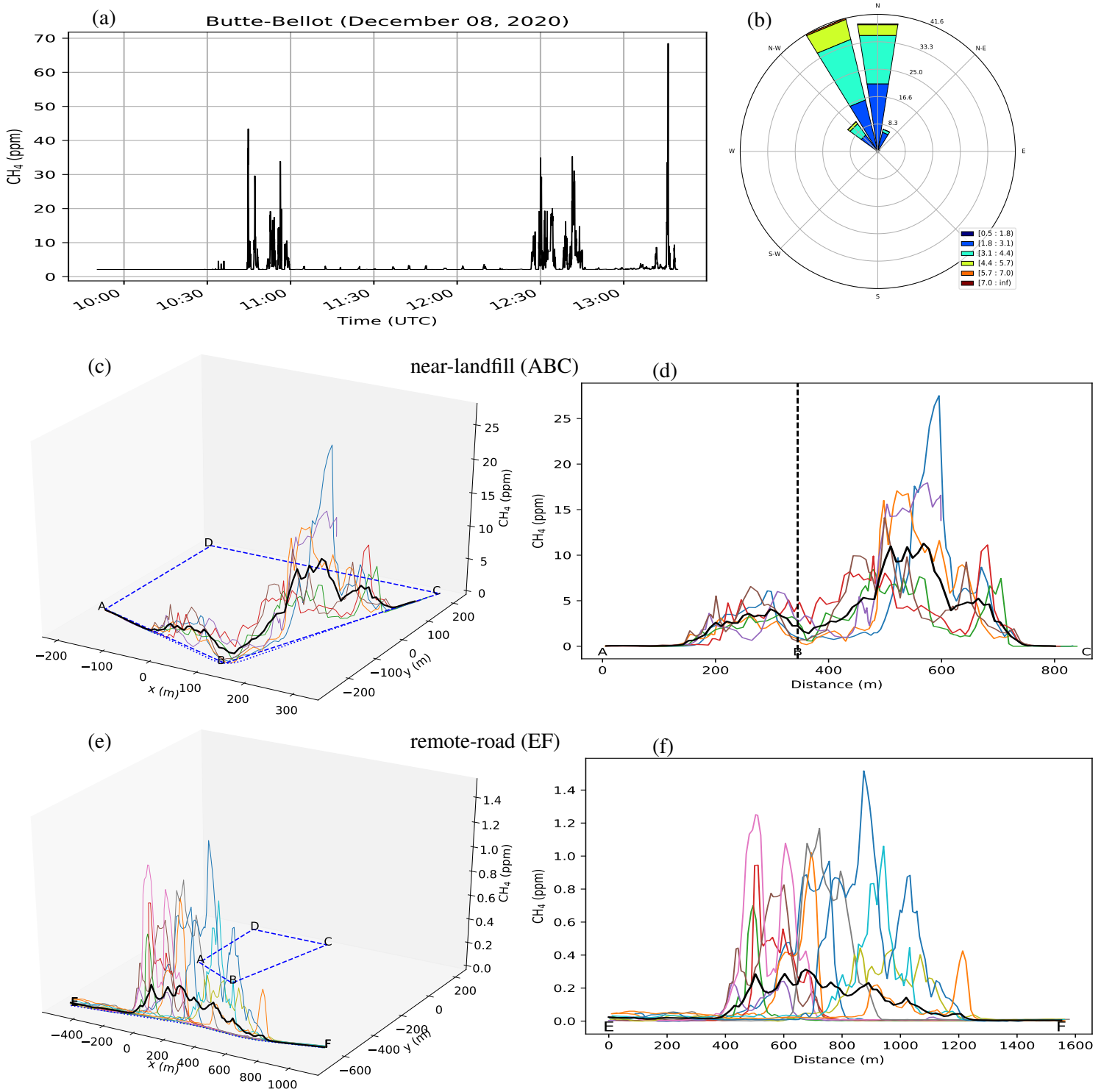

Figure S1.22. (a) CH_4mole fraction time series from the mobile near-surface measurements and (b) wind rose on **December 08, 2020**. Enhancement of CH_4mole fractions above the background in plume transects (c) & (d) along the near-landfill (ABC) road and (e) & (f) far-landfill remote road (EF). The distances along road segments are computed from A and E respectively for near-landfill (ABC) and far-landfill (EF) roads. Black lines in (c)-(f) show the averaged mole fractions computed from these multiple transects.